NUMERICAL SIMULATION OF THE FORMATION AND THE DRIPPING OF DROPLET IN THE ELECTROSLAG REMELTING PROCESS

by

Shuang LIU[a], Zhu HE[a*], Cai HUI[a], Qiang WANG[b], and Baokuan LI[b]

[a] State Key Laboratory of Refractories and Metallurgy,
Wuhan University of Science and Technology, Wuhan, China
[b] School of Materials and Metallurgy, Northeastern University, Shenyang, China

Original scientific paper
https://doi.org/10.2298/TSCI141117070L

Based on the magnetohydrodynamic module of the commercial computational fluid dynamics software FLUENT, a 3-D mathematical model was developed to describe the multi-field coupling phenomenon in the electroslag remelting process. The model predicted value is in good agreement with the experimental measurements. The simulation results show that, during the melt dripping process, the resistance of the electroslag remelting system is decreasing while the current density and velocity, as well as the temperature are increasing gradually. The maximum value of current density, electromagnetic force, and velocity appears when the melt droplet detaches and the quality of large droplets fall into the slag-metal interface. The maximum value of the current density is increased by almost one order of magnitude. The maximum value of the electromagnetic force and velocity increased by 2.5 and 4.7 times, respectively. The maximum value of Joule heating and temperature appears when the droplets fall into the slag-metal interface. The maximum value of the Joule heating and temperature increased for about 174.7% and 26.8%, respectively, when compared with the moment of the melt droplet formation.

Key words: *electroslag remelting, magnetohydrodynamics, multi-field coupling, formation and dripping of the melt droplet*

Introduction

Electroslag remelting (ESR) is an advanced metallurgical technology for production of high quality special steel and alloy steel, which couples many phenomena such as, MHD and heat and mass transfer. The fine grained, high-purity ingot products are widely used in the production of turbine disks for aeronautical bearings, submarine shells, aircraft engines, gun steels, titanium alloys for astronautics, crank axles for ships, and high-speed tool steels.

In the ESR process, the alternating or direct current is passed from a conventionally cast electrode through the molten slag and the liquid metal pool to the ingot, as shown in fig. 1. Due to the high electrical resistivity of the slag, Joule heating is generated in the slag layer, which melts the electrode tip. The molten metal passes through the slag layer in the form of droplets, accumulates in the liquid metal pool and then solidifies directionally. The metallurgical properties of the ingot are directly related to the solidification process, which strongly depends on hydrodynamic and thermal condition in the liquid pool and the mushy zone, as well as the

* Corresponding author, e-mail: hezhu@wust.edu.cn

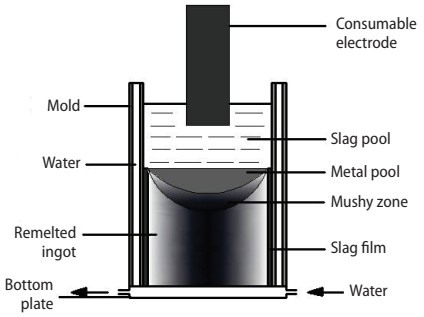

Figure 1. Schematic diagram of ESR

development of the heat and mass transfer at the slag/droplet interface. On the other hand, fluid flow, heat and mass transfer in the slag phase influence the electrode melting process and, thus, the energy efficiency of the operation. Therefore, a thorough understanding of the transport phenomena in the ESR system is needed to improve the control of the ESR process.

Due to the opaque nature of the slag and the metal phase, as well as the high temperature, experimental observation of the process is very difficult. More and more researchers have devoted significant efforts to develop the mathematical models for better understanding of the electromagnetic phenomenon, fluid flow, heat and mass transfer during the ESR process. Mitchell and Joshi [1] developed the mathematical models to predict the voltage distribution within the slag. Lately, Li *et al.* [2] developed a 3-D finite element model for the ESR system and obtained good agreement between the computed results and the measurement. Based on the finite difference technique, the general model have been developed for analyzing the electromagnetic fields, fluid flow and heat transfer in ESR [3]. The effects of electromagnetic force, natural convection, momentum, and heat transfer by the moving droplets were thoroughly investigated. However, the interface between the slag-pool and pool-ingot were assumed to be flat. In addition, the influence of the droplets was taken into account in the form of a momentum and energy source applied to slag and pool regions [4-10]. These simplifying assumption restrict the further application of the aforementioned models. Kharicha *et al.* [11] have showed that the slag/steel interface is never flat and may even become unstable. Recently, models fully coupled the MHD and the multiphase flow fields have been used successfully to solve 2-D problems related to the ESR process [12].

Thus, it is fundamentally important to study how the droplets forms and behaves in the ESR system and their effects on electromagnetic fields, fluid flow, as well as heat and mass transfer. The purpose of the current research is to report on numerical investigation, which have been undertaken to study the unsteady distribution of current, electromagnetic force, velocity, and temperature filed based on the 3-D MHD model coupled with a volume of fluid (VOF) model for the phases distribution.

The numerical model

In the development of a mathematical statement of this problem, the following conservation equations of fluid flow and electromagnetic force field, as well as the heat transfer have to be considered. The coupled nature of these equations is readily apparent, in which the temperature field affects the fluid flow equations through the buoyancy term, and the knowledge of the velocity field and of the turbulence parameters is required in the solution of the convective heat transfer equation. The geometrical parameters, Physical properties of the metal and slag, as well as the process parameters are list in tab. 1-3.

Table1. Geometrical parameters

Geometry	Value
Electrode diameter [m]	0.057
Immersion depth of electrode [m]	0.02
Slag height [m]	0.07
Mold diameter [m]	0.10

Governing equations

This model is based on the numerical solution of the Maxwell, Navier-Stokes, and convective heat balance equations. It is assumed that the ef-

Table 2. Physical properties of the metal and slag

Properties	Slag	Metal
Density [kgm^{-3}]	2800	7200
Viscosity [kgm^{-1}s^{-1}]	0.015	0.006
Liquidus temperature [K]	1650	1723
Solidus temperature [K]	1550	1573
Specific heat [Jkg^{-1}K^{-1}]	1246	753
Thermal conductivity [Wm^{-1}K^{-1}]	11	15.48
Electric conductivity [Ω^{-1}m^{-1}]	250	714000
Latent heat [kJkg^{-1}]	518	247

Table 3. Process parameters

Conditions	Value
Interfacial tension [Nm^{-1}]	0.9
Voltage [V]	40
Emissivity of free slag surface	0.6
Heat transfer at the slag-air wall [Wm^{-2}K^{-1}]	100
Heat transfer at the slag-mold wall [Wm^{-2}K^{-1}]	272
Heat transfer at the meta-mold wall [Wm^{-2}K^{-1}]	350

fects of the electrode movement are neglected, which is valid for the slag and the upper part of the ingot once the ingot height reaches the order of magnitude of the ingot diameter [13].

The equation of continuity for incompressible fluid is:

$$\nabla\vec{\mathrm{u}} = 0 \tag{1}$$

and the equation of motion is given:

$$\frac{\partial}{\partial t}\left(\rho\vec{\mathrm{u}}\right) + \nabla\left(\rho\vec{\mathrm{u}}\vec{\mathrm{u}}\right) = -\nabla p + \mu_{\mathrm{eff}}\nabla^2\vec{\mathrm{u}} + \vec{\mathrm{F}}_b + \vec{\mathrm{F}}_e \tag{2}$$

where $\vec{\mathrm{u}}$ is the velocity of the flow, ρ – the density of the fluid, and p – the pressure. The turbulent viscosity, μ_{eff}, is obtained with the aid of the RNG k-ε model. The $\vec{\mathrm{F}}_b$ represents the effects of buoyancy force determined by the Boussinesq approximation and $\vec{\mathrm{F}}_e$ is the Lorenz force.

The energy equation of the enthalpy-porosity formulation is:

$$\frac{\partial}{\partial t}\left(\rho H\right) + \nabla\rho\vec{\mathrm{u}}H = \nabla\left(k_{\mathrm{eff}}\nabla T\right) + Q_{\mathrm{Joule}} \tag{3}$$

where H is the enthalpy of the metal and the slag which is the sum of the sensible enthalpy and the latent heat released in the mushy zone:

$$H = h + f_l L \tag{4}$$

$$h = h_{\mathrm{ref}} + \int_{T_{\mathrm{ref}}}^{T} c_p \mathrm{d}T \tag{5}$$

where f_l is the liquid fraction and defined:

$$f_l = \frac{T - T_s}{T_l - T_s} \tag{6}$$

where T_s and T_l are solidus and liquidus temperature, respectively.

The mathematical formulation of the electric and magnetic field is composed of the Maxwell's equations, Lorenz law, and Joule law.

$$\nabla\times\vec{\mathrm{H}} = \vec{\mathrm{J}} \tag{7}$$

$$\nabla\times\vec{\mathrm{E}} = -\frac{\partial\vec{\mathrm{B}}}{\partial t} \tag{8}$$

$$\nabla \cdot \vec{B} = 0 \tag{9}$$

$$\vec{B} = \mu_0 \vec{H} \tag{10}$$

$$\vec{F}_e = \vec{J} \times \vec{B} \tag{11}$$

$$Q_{\text{Joule}} = \frac{1}{\sigma} \vec{J} \cdot \vec{J} \tag{12}$$

where $\vec{H}$ is the magnetic field, $\vec{J}$ – the current density, $\vec{E}$ – the electric field, $\vec{B}$ – the magnetic flux density, μ_0 – the magnetic permeability, and σ – the electric conductivity.

The metal/slag interface is tracked with the VOF method which follows conservation equation:

$$\frac{\partial \alpha}{\partial t} + \nabla\left(\alpha \vec{u}\right) = 0 \tag{13}$$

The mushy zone is treated as a *pseudo* porous medium through the enthalpy-porosity formulation in which the porosity decreases from 1 to 0 as the metal solidifies. The liquid fraction in each cell is set to the porosity in that cell.

Boundary conditions

At the inlet the melting rate obtained from experiment is imposed and outflow is applied on the outlet. The no-slip condition is applied on the wall where the slag and metal are in contact with the mold. Along the exposed slag surface, a zero shear condition is assumed for the radial velocity. For the electromagnetic field, zero potential is applied on inlet and a corresponding potential gradient is applied on outlet. The mold lateral wall is assumed to be an insulating wall. The top surface of slag as well as the mold wall is supposed to exchange heat with the surrounding air by natural convection and thermal radiation.

Solution method

The electromagnetic field is obtained by the electrical potential method [14] which simultaneously solve the electric potential, φ, as well as magnetic potential vector, $\vec{A}$, equations. A control volume-based technique was used to convert the non-linear governing equations to algebraic equations that can be solved numerically. The SIMPLE algorithm was applied for the pressure-velocity coupling. A segregated and implicit solver was used to solve the governing equations and the second-order accuracy central differencing scheme was adopted to improve the accuracy of the solution. The commercial finite volume CFD code, FLUENT was used to compute the two-phase flow, heat transfer, and solidification and the MHD model coupled user defined functions was employed to describe the electromagnetic phenomena. The electric current distribution is dynamically adapted to the transient phase distribution and then the electromagnetic forces and the Joule heating are recalculated at each time step, which are incorporated into the momentum and energy equation as a source term, respectively. The mesh is refined to the point where further refinements will not induce noticeable change (not more than 5%) in results. The convergence criterion for scaled residuals was set to be less than 10^{-6}. The computational model and mesh are shown in fig. 2.

Results and discussion

Figure 3 shows a comparison between the experimentally measured axial temperature profiles at radial position $r = 2.5$ cm and those predicted from the present numerical model. The discrete data points denote measurements and the line denotes predictions for the condition. The computed values are in good agreement with measurement and the deviation between the experiment and computation is less than 5%, which proves the accuracy of the present mathematical model.

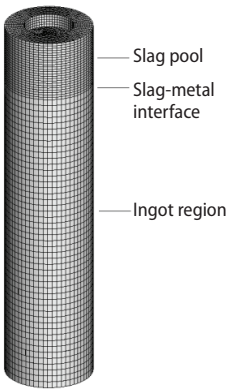

Figure 2. Computational model and mesh

In figs. 4(a)-(d), the representative snapshots of the droplet dripping during the ESR process are shown at four different instants. There, the first figure corresponds to an instant immediately following the initial formation of the metal droplet due to the temperature rising and melting of the electrode tip. In fig. 4(b), the metal droplet is enlarged and necking phenomenon occurs. Due to the joint effects of the gravity, Lorentz force and surface tension, the metal droplet begins to detach from the electrode tip, as shown in fig. 4(c). In fig. 4(d), most of the metal has entered in the liquid metal pool, accompanied with the perturbations of the slag/metal interface. The moment corresponding to figs. 4(a)-(d) will be referred as T_a, T_b, T_c, and T_d in the following content, respectively.

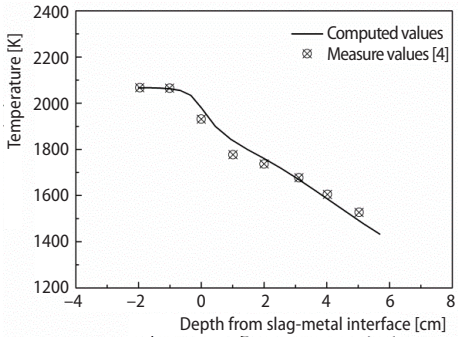

Figure 3. Computed and measured axial temperature at $r = 2.5$ cm

The presence of two phases in the present work makes the local value of the electrical conductivity vary in time and space. The distribution of the electric current coming from the top electrode is controlled by the distribution of the phase fraction, that is, the movement of the metal droplet, as shown in figs. 5(a)-(d), on which the volume fraction of the metal is superimposed. Because of the high conductivity of the metal droplet, most electrical current flows following the metal droplet, rather than through the slag. With the electrode melting, the metal droplet becomes larger and larger, the total resistance of ESR system decreases correspondingly during the process of metal droplet formation and dripping. When the metal droplets pass through the slag layer and entering into the metal pool, the volume fraction of the molten metal is small and the current density decrease.

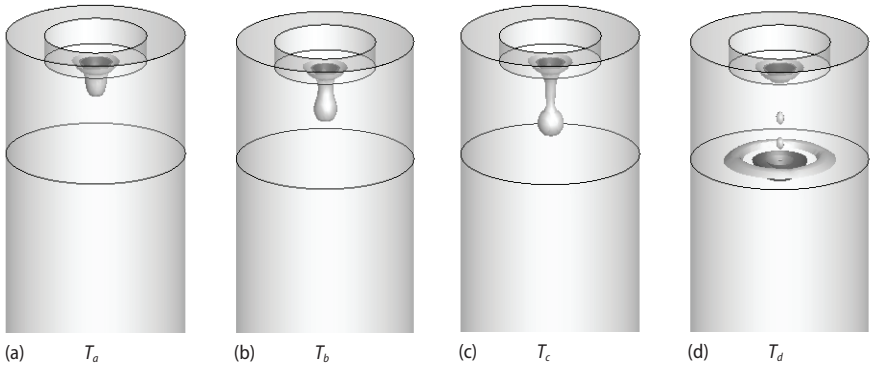

Figure 4. The shape of droplet at different time instant

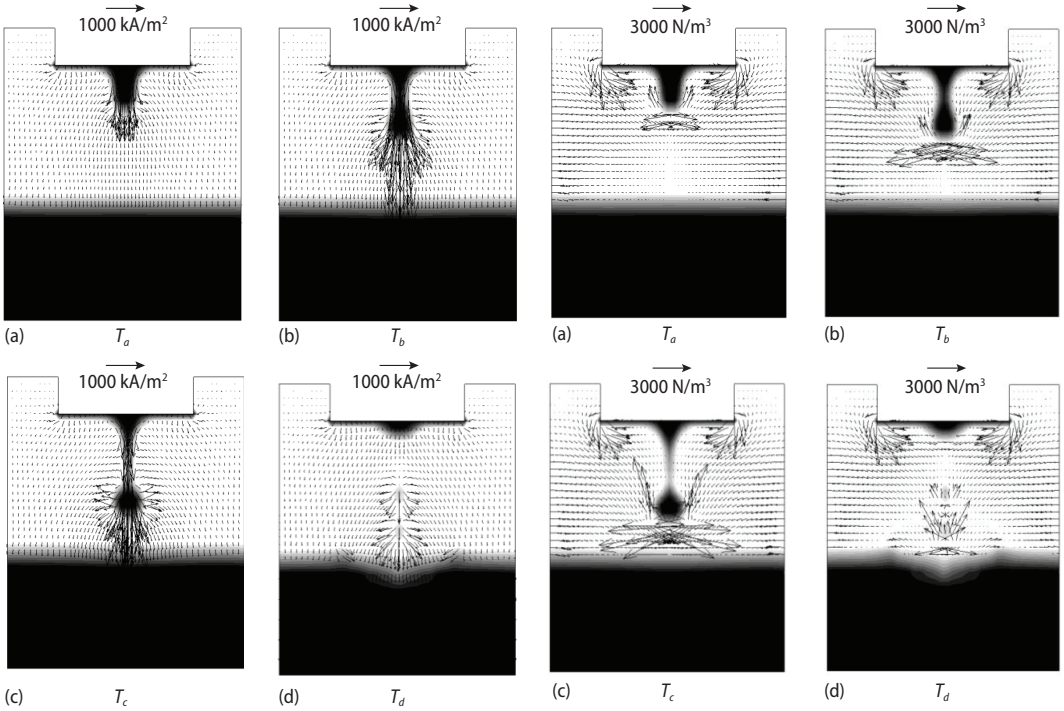

Figure 5. Current density distribution of ESR system at different time instant

Figure 6. Electromagnetic force field distribution of ESR system at different time instant

The distributions of the Lorentz force at different instant are shown in figs. 6(a)-(d) with the volume fraction of the metal superimposed. The Lorentz force is produced by an interaction of the oscillating current and magnetic fields. In most of the metal region, the Lorentz force is radially inwards and the presence of the metal droplet have strong effects on the distribution of the Lorentz force. The direction of the Lorentz force imposed on the metal droplet is opposed to that of its movement, and the Lorentz force continuously increases as the metal droplet grows.

One of the roles of the slag in ESR is to produce the necessary Joule heating to melt electrode. The Joule heating per unit volume is determined from the current density and inversely proportional to the electrical conductivity of slag, hence ESR slag with lower electrical conductivity would provide higher Joule heating to melt the electrode. Figures 7(a)-(d) shows the contours of the Joule heating produced by the current as different instant. The Joule heating is concentrated especially at the location of the metal droplet. Further, near the *corner* of the electrode in the slag and just under the slag/metal interface, the Joule heating are also enhanced.

The temperature distribution in ESR system plays an important role to the organization and the quality of the ingot. Unlike the distribution of Joule heating, the temperature distribution in the slag layer and metal pool is the results of interaction between the productions of Joule heating and the metal droplet movements. The Joule heating carried by the metal droplet can be transferred to the region around them and the slag is hottest on the two sides beneath the electrode. It can also be seen that very large temperature gradients exist at the mold wall, as shown in figs. 8(a)-(d). At the moment of T_a, T_b, and T_c during the dripping of the metal droplet,

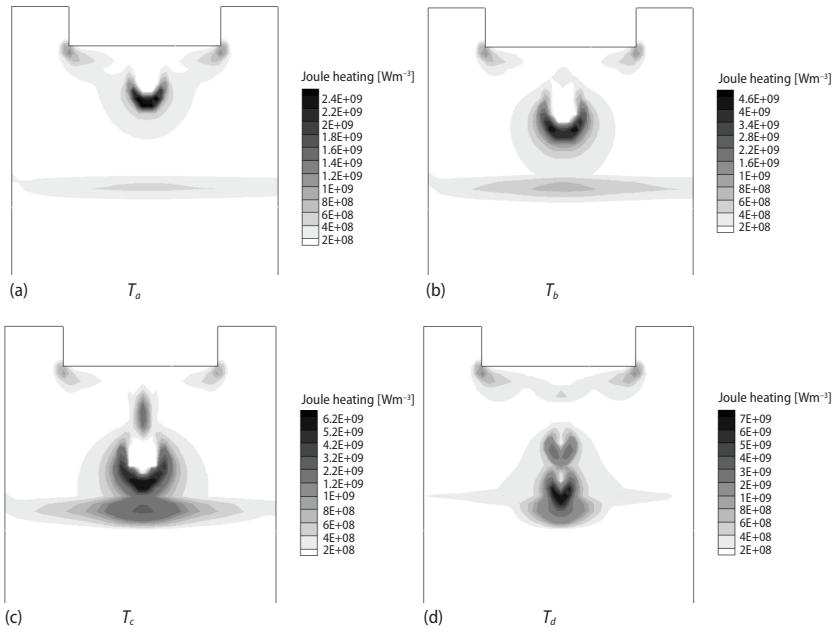

Figure 7. Joule heating field distribution of ESR system at different time instant

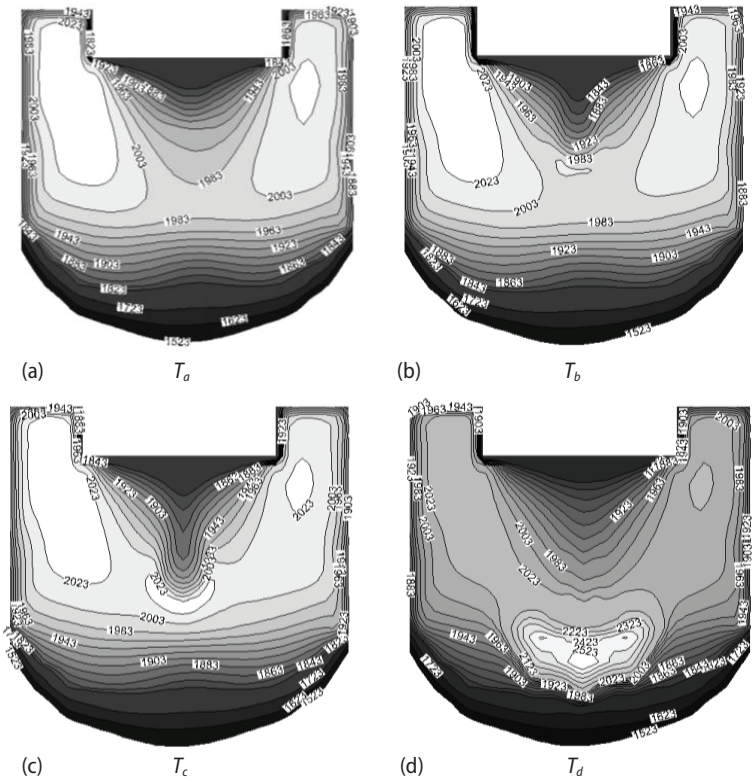

Figure 8. Temperature field distributions of ESR system at different time instant

the temperature just below the electrode tip is slightly lower than the highest temperature region. While, at the moment of T_d the temperature below the electrode tip is the highest.

In the slag phase, two symmetrical re-circulating cells are observed and these two vortices, is induced by electromagnetic forces, as shown in figs. 9(a)-(d). Beneath the electrode, some instabilities of a Rayleigh-Benard type arise because of Joule heating and cooling by contact with the electrode tip.

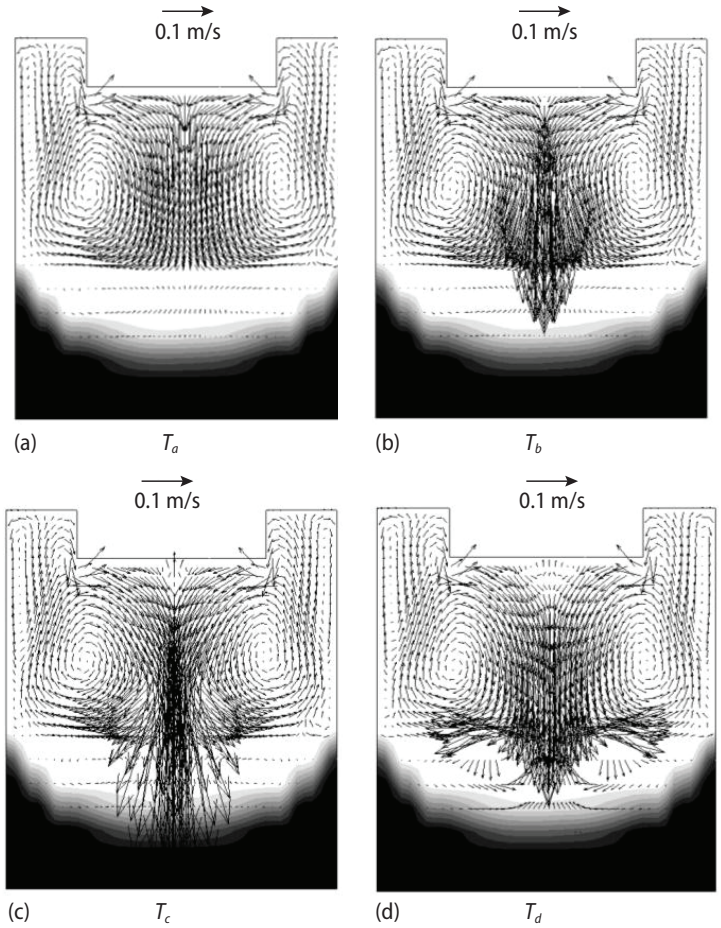

Figure 9. Velocity field distributions of ESR system at different time instant

Conclusions

A 3-D mathematical model coupled with MHD model has been developed to investigate the two-phase flow behavior during the ESR process, in which the electromagnetic forces and the Joule heating are recalculated at each time step, which are incorporated into the momentum and energy equation as a source term, respectively. This model has been used to investigate the droplet formation and dripping as well as the corresponding electromagnetic field, velocity field and temperature field. The model predicted value is in good agreement with the experimental measurements in literature. The simulation results show that, during the melt dripping process, the resistance of ESR system is decreasing while the current density and velocity, as well as the temperature are increasing gradually. The maximum value of current density, elec-

tromagnetic force and velocity appears when the melt droplet detaches and the large droplets fall into the slag-metal interface. The maximum value of the current density is increased by almost one order of magnitude. The maximum value of the electromagnetic force and velocity increased by 2.5 and 4.7 times, respectively. The maximum value of Joule heating and temperature appears when the droplets fall into the slag-metal interface. The maximum value of the Joule heating and temperature increased for about 174.7% and 26.8% when compared with the moment of the melt droplet formation.

Acknowledgement

This work was supported by the Natural Science Foundation of China (51210007, 51404176) and the Opening Project of State Key Laboratory of Refractories and Metallurgy of Wuhan University of Science and Technology (No. G201606).

Nomenclature

$\vec{A}$ – magnetic potential vector, [Vsm^{-1}]
$\vec{B}$ – magnetic flux density, [T]
c_p – specific heat at constatnt pressure, [Jkg^{-1}K^{-1}]
$\vec{E}$ – electric field intensity, [Vm^{-1}]
$\vec{F}_b$ – buoyancy force, [Nm^{-3}]
$\vec{F}_e$ – Lorentz force, [Nm^{-3}]
f_l – liquid fraction
H – enthalpy of the metal and the slag, [J]
$\vec{H}$ – magnetic field intensity, [Am^{-2}]
h – sensible enthalpy, [J]
$\vec{J}$ – current density, [Am^{-2}]
k_{eff} – effective thermal conductiviy, [Wm^{-1}K^{-1}]
L – latent heat of fusion, [Jkg^{-1}]
p – pressure, [Pa]
Q_{Joule} – Joule heating, [Wm^{-3}]
r – radius of the electrode, [m]
T – temperature, [K]
T_l – liquidus temperature, [K]
T_s – solidus temperature, [K]
t – time, [s]
$\vec{u}$ – velocity, [ms^{-1}]
x, y, z – Cartesian co-ordinates

Greek symbols

α – volume fraction of metal
μ_{eff} – turbulent viscosity, [Pa·s]
μ_0 – vacuum permeability, [Hm^{-1}]
ρ – density of fluid, [kgm^{-3}]
σ – electric conductivity, [Ω^{-1}m^{-1}]
φ – electric potential, [Vm^{-1}]

References

[1] Mitchell, A., Joshi, S., The Thermal Characteristics of the Electroslag Process, *Metallurgical Transactions*, *4* (1973), 3, pp. 631-642
[2] Li, B. K., *et al*., Current Magnetic Field and Joule Heating in Electroslag Remelting Processes, *ISIJ International*, *52* (2012), 7, pp. 1289-1295
[3] Dilawari, A. H., Szekely, J., A Mathematical Model of Slag and Metal Flow in the ESR Process, *Metallurgical Transactions B*, *8* (1977), 1, pp. 227-236
[4] Choudhary, M., Szekely, J., The Modeling of Pool Profiles, Temperature Profiles and Velocity Fields in ESR Systems, *Metallurgical Transactions B*, *11* (1980), 3, pp. 439-453
[5] Choudhary, M., Szekely, J., The Effect of Temperature Dependent Electrical Conductivity on Flow and Temperature Fields in Slags in ESR Systems, *Metallurgical Transactions B*, *12* (1981), 2, pp. 418-421
[6] Choudhary, M., *et al*., The Velocity Field in the Molten Slag Region of ESR Systems: A Comparison of Measurements in a Model System with Theoretical Predictions, *Metallurgical Transactions B*, *13* (1982), 1, pp. 35-43
[7] Dilawari, A. H., Szekely, J., Heat Transfer and Fluid Flow Phenomena in Electroslag Refining, *Metallurgical Transactions B*, *9* (1978), 1, pp. 77-87
[8] Dilawari, A. H., *et al*., Electromagnetically and Thermally Driven Flow Phenomena in Electroslag Welding, *Metallurgical Transactions B*, 9 (1978), 3, pp. 371-381
[9] Jardy, A., *et al*., Magnetohydronamic and Thermal behavior of Electroslag Remelting Slags, *Metallurgical Transactions B*, *22* (1991), 1, pp. 111-120

[10] Mitchell, A., Hernandez-Morales, B., Electromagnetic Stirring with Alternating Current during Electroslag Remelting, *Metallurgical Transactions B*, *21* (1990), 4, pp. 723-731
[11] Kharicha, A., *et al*., Shape and Stability of the Slag/Melt Interface in a Small DC ESR Process, *Materials Science and Engineering: A*, *413* (2005), Dec., pp. 129-134
[12] Weber, V., *et al*., A Comprehensive Model of the Electroslag Remelting Process: Description and Validation, *Metallurgical and Materials Transactions B*, *40* (2009), 3, pp. 271-280
[13] Ballantyne, A. S., Mitchell, A., Modeling of Ingot Thermal Fields in Consumable Electrode Remelting Process, *Ironmaking Steelmaking*, *4* (1977), 4, pp. 222-239
[14] Biro, O., Preis, K., On the Use of the Magnetic Vector Potential in the Finite-Element Analysis of Three-Dimensional Eddy Currents, *IEEE Transactions on Magnetics*, *25* (1989), 4, pp. 3145-3159

Paper submitted: November 17, 2014
Paper revised: March 29, 2015
Paper accepted: April 22, 2015

© 2017 Society of Thermal Engineers of Serbia
Published by the Vinča Institute of Nuclear Sciences, Belgrade, Serbia.
This is an open access article distributed under the CC BY-NC-ND 4.0 terms and conditions